Video Article

A Microfluidic Platform for Precision Small-volume Sample Processing and Its Use to Size Separate Biological Particles with an Acoustic Microdevice

Erika J. Fong[1,2], Chao Huang[1], Julie Hamilton[1], William J. Benett[1], Mihail Bora[1], Alison Burklund[1], Thomas R. Metz[1], Maxim Shusteff[1]

[1]Materials Engineering Division, Lawrence Livermore National Laboratory

[2]Department of Biomedical Engineering, Boston University

Correspondence to: Maxim Shusteff at shusteff1@llnl.gov

URL: http://www.jove.com/video/53051
DOI: doi:10.3791/53051

Keywords: Bioengineering, Issue 105, microfluidics, lab on a chip, cell separation, acoustophoresis, lab automation, microfabrication, MEMS, LabVIEW

Date Published: 11/23/2015

Citation: Fong, E.J., Huang, C., Hamilton, J., Benett, W.J., Bora, M., Burklund, A., Metz, T.R., Shusteff, M. A Microfluidic Platform for Precision Small-volume Sample Processing and Its Use to Size Separate Biological Particles with an Acoustic Microdevice. *J. Vis. Exp.* (105), e53051, doi:10.3791/53051 (2015).

Abstract

A major advantage of microfluidic devices is the ability to manipulate small sample volumes, thus reducing reagent waste and preserving precious sample. However, to achieve robust sample manipulation it is necessary to address device integration with the macroscale environment. To realize repeatable, sensitive particle separation with microfluidic devices, this protocol presents a complete automated and integrated microfluidic platform that enables precise processing of 0.15–1.5 ml samples using microfluidic devices. Important aspects of this system include modular device layout and robust fixtures resulting in reliable and flexible world to chip connections, and fully-automated fluid handling which accomplishes closed-loop sample collection, system cleaning and priming steps to ensure repeatable operation. Different microfluidic devices can be used interchangeably with this architecture. Here we incorporate an acoustofluidic device, detail its characterization, performance optimization, and demonstrate its use for size-separation of biological samples. By using real-time feedback during separation experiments, sample collection is optimized to conserve and concentrate sample. Although requiring the integration of multiple pieces of equipment, advantages of this architecture include the ability to process unknown samples with no additional system optimization, ease of device replacement, and precise, robust sample processing.

Video Link

The video component of this article can be found at http://www.jove.com/video/53051/

Introduction

Sample separation and fractionation is one of the most promising areas of application for microfluidic technologies. Such sample handling steps are integral for effective clinical diagnostics, therapeutics development, biosurveillance efforts, and progress in life science research and technology. A myriad microfluidic separation strategies have been demonstrated for fluid-suspended particulates and colloids, as well as for chemical and biological species; several reviews provide overviews of recent progress and developments in these fields[1–9]. Although many of these microfluidic separation technologies (hereafter referred to as “Core Devices”) have been extensively characterized, few reports have considered the sample separation problem at a system level. The Core Devices are typically individual centimeter-scale chips, interfaced to fluoropolymer tubing, with fluid delivered by a displacement or pressure pump. Yet, if the promise of microfluidics—including increased automation, reliability, and reduction in sample volumes—is to become reality, at least an equivalent effort must be devoted to the design of a complete separation system into which the Core Device is integrated.

In addition, a major challenge for microfluidic approaches to biodetection is the macro to micro interface. This refers not only to the physical “world-to-chip” connections of a microfluidic device to macroscale components, and to the mismatch between typical clinical or analytical sample volumes (~0.1–10 ml) and the internal volume of microfluidic chips (~0.01–10 µl), but also to the statistical sampling limitations arising from bridging these size scales. These issues contribute to the perception that sample pre-processing and preparation are the “weak link” of biodetection.[10] The platform described in this work takes major steps toward addressing these challenges.

Taking a system-level view, this protocol details the reliable processing of precisely-metered analytical-scale volumes (ranging from 0.15 to 1.5 ml) on ~10-min timescales. This is a “one-button” operation: once the source vial containing the sample and destination vials for fraction collection are placed into the system, the “run” command initiates the procedure, and all steps are computer-controlled. At the end of a run, the collection vials can be removed from the system for downstream analysis of the separated fractions.

The Core Device in this system is an acoustophoresis chip which extracts mammalian cell-sized (5–20 µm) particles from the sample. Acoustophoretic separation is chosen here primarily because it is high-throughput (up to 100s of µl/min), label-free, and non-contact, thus offering advantages in separating viable viruses from cells that few other microfluidic techniques can match. The physics of acoustic particle

focusing have been extensively described,[11–13] and are not the focus of this protocol, but a brief summary of the underlying concepts follows to aid in understanding the application to microfluidic separation.

Ultrasound standing waves resonating in fluid-filled microchannels produce pressure fields, which give rise to forces that drive particles toward nodes of low pressure. The force magnitude depends on the particle's volume, and on an acoustic contrast factor derived from the relative densities and compressibilities of the particle and the suspending fluid.[14] As such, acoustic focusing is ideally suited to separation of cell-sized (~7–15 µm) from virus-sized (~50–200 nm) particles. The larger particles migrate toward a pressure node; however, since the force magnitude is very small for particles smaller than 2–3 µm, these small particles or dissolved species hardly move at all. Our specific implementation of acoustic separation, as previously described,[15] incorporates a thin wall to subdivide the fluid channel and allows tunable, asymmetric placement of the focusing position. This adds flexibility in device design, and the performance benefits—including increased separation quality and speed—are fully described elsewhere.[16,17]

However, a major advantage of the system-level design approach described in this work is that it is adaptable to a great variety of microfluidic Core Devices. For example, most other continuous-flow separation modes, including inertial, flow-field fractionation, deterministic lateral displacement (DLD), and various types of electrokinetic devices can be readily incorporated, with appropriate adjustments made to account for changes in inlet/outlet configuration, flow rates, and sample volumes. Devices with various types of on-chip fields (electric, magnetic) or gradients (thermal, chemical) may require additional connections to the chip, or the integration of additional hardware, which this platform accommodates.

This protocol provides the steps required to design a microfluidic separation device, and to fabricate silicon-glass chips by deep reactive ion etching (DRIE, a plasma-etch process available in many microfabrication facilities, which uses alternating cycles of etching and passivation to achieve deep features with vertical sidewalls[18]). Next, we describe the characterization of the acoustofluidic device to determine the optimal operating parameters for separation, and finally detail the fully-integrated separation system and the procedure for processing biological samples. Typical device characterization results and sample processing data are then presented and discussed, and the key advantages of this approach are highlighted, including modularity, robustness, precision and automation.

Protocol

1. Acoustophoretic Device Design and Photomask Layout

NOTE: General considerations and guidance for microfabrication process design and mask layout can be found in texts on microfabrication and tutorials of photomask design.[19–21]

1. Lay out Mask 1, the Fluidic Layer (front side), using appropriate CAD software. Choose a geometry that permits sample injection and separation appropriate for the desired application.
    1. For acoustic focusing, set the fluidic channel width w to provide a resonant frequency f_n greater than 1 MHz according to the equation $f_n = nc/2w$, where c is the speed of sound in the relevant fluid and n is the number of standing-wave nodes (*e.g.*, for a 900-µm wide channel, the two-node resonance is expected at f_2 = 1.65 MHz).
    NOTE: Particles occupying distinct lateral positions near the end of the separation channel should exit from distinct outlets. In this protocol, particles are separated by size, so the outlets are designated SPO and LPO, for small-particle and large-particle outlet, respectively, as shown in **Figure 1**.
    2. Set the fluid channel length to control the length of time particles are exposed to the separation field at a specific flow rate. Longer on-chip residence time for particles to migrate due to separation forces must be traded off against the larger required chip footprint.
    NOTE: In our acoustic focusing devices, the flow channel makes three passes down the chip for increased residence time (**Figure 2a**). At a typical total flow rate of 200 µl/min, particles flowing through the 300 x 200 µm cross-section, 117-mm long separation channel spend on average 2.1 sec in the acoustic field.
2. Include fluidic ports in the mask layout for connections to standard tubing arranged on a standardized grid (5-mm pitch). Include suitable fiducial marks for alignment of masks to each other during fabrication and dicing of individual devices.
3. Lay out Mask 2, the Via Layer (back side), which only includes fluidic ports. Include fiducial marks for alignment to Mask 1.

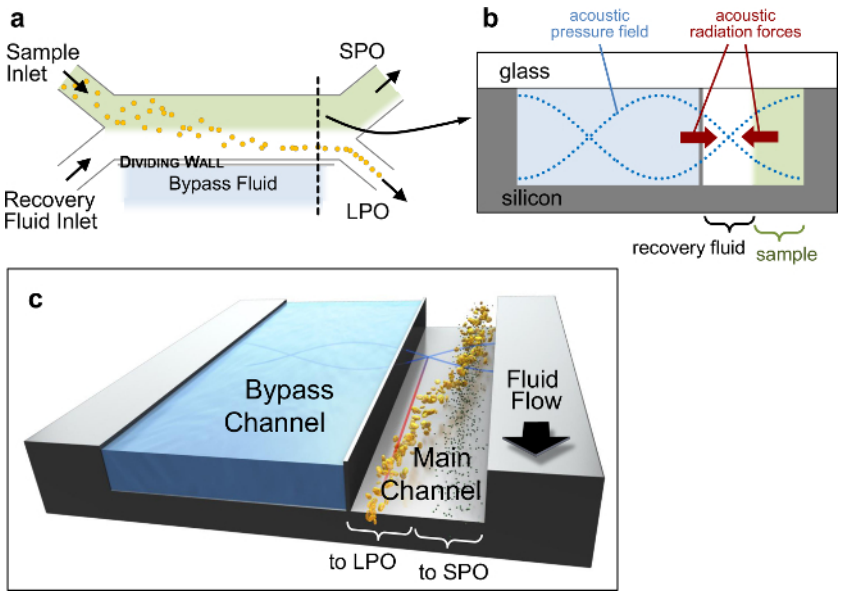

Figure 1. Acoustofluidic Device. Schematic sketches of acoustophoretic device architecture. (**a**) Top view, showing the overall H-filter configuration (not to scale). (**b**) Schematic of the channel cross-section at the location marked by the black dashed line in (a), showing the pressure field (blue dotted lines), and the sense of the acoustic primary radiation forces (PRF) that drive particles toward nodal planes (red arrows). The channel cross-section is 900×200 µm with a wall approximately 10 µm thick separating the main (300 µm wide) and bypass channels. (**c**) 3D representation of particle separation. Please click here to view a larger version of this figure.

2. Cleanroom Fabrication of Microfluidic Chips for Acoustophoresis

1. Pattern the back-side fluid ports using Mask 2 on a double-side polished 0.5-mm thick, 100-mm diameter <100> silicon wafer by standard positive-resist photolithography. Etch this geometry by deep reactive ion etching (DRIE) to a depth of 350–400 µm.
2. Turn the wafer over, and pattern the front-side fluid channel geometry using Mask 1 by standard positive-resist photolithography onto the other side of the silicon. Then, mount the device wafer to a second (blank silicon) carrier wafer using photoresist.
3. Etch the channels, also by DRIE, to a depth of 200 µm, through-etching the silicon in the port locations (the carrier wafer protects the DRIE tool surface). De-mount the device wafer from the blank Si wafer by soaking in resist-stripping solution.
4. Clean the device wafer and a featureless 0.5 mm-thick borosilicate glass wafer using Piranha solution (sulfuric acid and hydrogen peroxide in a 3:1 ratio).
5. Seal the fluid channels by anodically bonding the glass and silicon wafers using the following parameters: chamber pressure at 3 mTorr, piston pressure at 1,000 N, temperature at 350 °C, and apply 750 V until the current drops below 0.2 mA.
6. Cut the individual chips apart with a diamond blade on a dicing saw.

3. Final Device Assembly

1. Piezo Transducer Attachment
   NOTE: Ultrasound is generated in the microfluidic chip by a piezoceramic transducer attached to the silicon side.
   1. From a two-component low-viscosity epoxy kit, weigh out the recommended ratio of both components and mix them thoroughly.
   2. Dispense the epoxy mixture with a pipette and spread evenly across a lead zirconate titanate (PZT) piezoceramic to create a thin, even layer (approximately 10 µl of epoxy mixture for a piezo with dimensions of 37.5 × 10 × 0.5 mm).
   3. Using a suitable jig or fixture, align the epoxy side of the piezoceramic with the microfluidic chip, providing an overhanging area on one side for subsequent wire attachment (see **Figure 2a**), and bring the two components into contact. Clamp the assembly in a vice, taking care not to crack any of the components, and cure at the temperature and duration recommended by the epoxy manufacturer.
   4. After the epoxy has cured, attach fine-gauge wire leads to each side of the piezoceramic, by soldering with a fine-tip soldering iron, making the briefest possible contact with the piezo to avoid thermally de-polarizing it. Alternatively, use a conductive adhesive to glue wires to the piezo.

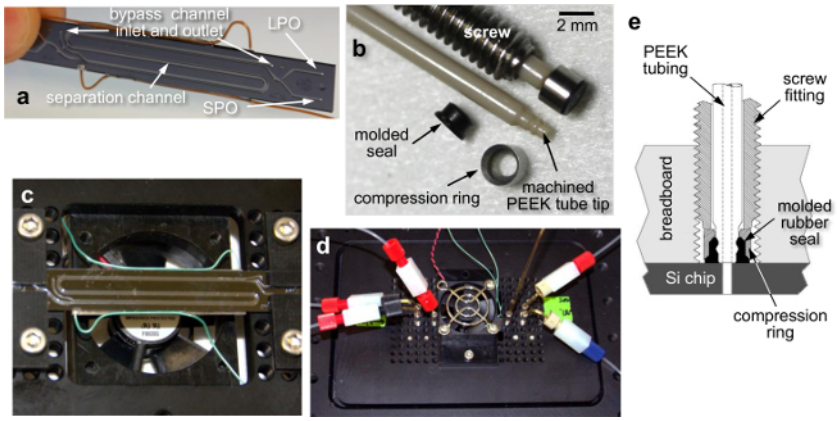

Figure 2. Fluidic Breadboard, Chip Mounting, and World-to-Chip Interface. Photos of (**a**) the acoustic microfluidic chip (external dimensions of 70×9×1 mm) with attached piezo transducer wire leads, showing three passes of the separation channel down the chip, (**b**) custom fluidic screw fittings and machined tubing components for the chip-to-world interface, (**c**) the chip mounted to the underside of the fluidic breadboard using clamping fixtures, spanning an opening in the breadboard to allow fan cooling, (**d**) a top view of the breadboard with attached tubing connections and cooling fan, and (**e**) a cross-sectional schematic of the screw fittings that interface the tubing with the mounted microfluidic chip. Please click here to view a larger version of this figure.

2. Device Mounting and World-To-Chip Interfacing
    1. Attach the chip to the “fluidic breadboard” (a plate with a grid of regularly-spaced threaded through-holes) using clamping fixtures. Attach a cooling fan to the breadboard to regulate temperature during acoustic experiments (see **Figure 2**).
    NOTE: Operating without the cooling fan at typical drive voltages raises the device temperature to 70–80 °C. This significantly shifts the resonant frequency due to altered sound velocity in the fluid, and may negatively impact the viability of any biological particles that are being processed.
    2. Screw in chip-to-world connectors, previously described elsewhere[22] and shown in **Figure 2**. Join these interface tubes to additional tubing at the inlets and outlets using standard ¼”-28 unions for 1/16” tubing.

4. Characterization of Acoustic Focusing Performance

NOTE: System components required for acoustic focusing characterization are grouped together in the Materials List. Steps 4.1 and 4.2 below apply to any Core Device used with this platform, whereas subsequent steps describe operations specific to the acoustofluidic device discussed here.

1. System Configuration
    1. Assemble the microfluidic chip using world-to-chip connections on the fluidic breadboard, as described in Section 3. Make connections using tubing (such as 1/16” outer diameter fluoropolymer tubing) to a fluid pump and collection vials. Mount the breadboard assembly on the stage of a microscope capable of fluorescence imaging equipped with a CCD camera.
    2. Connect lengths of small inner diameter (ID) tubing (0.006” is recommended) immediately after the chip (see **Figure 4**) to serve as flow restrictors, which stabilize the system and control the flow splitting between the chip outlets. Use larger ID tubes, such as 0.01” or 0.03”, for all other connections.
        1. Estimate the hydrodynamic flow resistance R_h of each piece of tubing with length L and inner diameter D using the equation $R_h = 128\ \mu L/\pi D^4$, where μ is the fluid’s dynamic viscosity. The pressure drop ΔP due to each length of tubing at a given flow rate Q is given by $\Delta P = QR_h$.
        2. Choose a ratio of restrictor lengths to split the flow between the outlets as appropriate for the separation method being used. Optimal separation with the acoustic chips in this protocol requires an SPO:LPO flow ratio of approximately 65:35%.
        3. Choose the length of the outlet flow restrictors such that their fluidic resistance is at least 3–4 times larger than the total resistance in the rest of the system (appropriately summed in series or parallel). For the acoustophoresis device used in this work, tubing lengths of 35 and 65 cm for the LPO and SPO are suitable.
        NOTE: Careful consideration must be given to R_h of any microfluidic Core Device. For our acoustic focusing chip in this work, R_h is low due to its relatively large channel dimensions, so the connected tubing resistances easily exceed it. For devices with smaller channel dimensions, the chip’s resistance may dominate the rest of the system tubing, in which case design and control of on-chip channel R_h is an additional consideration during Step 1 of this protocol. Detailed design principles and guidelines are available in the literature.[23,24]

2. System Verification
    1. Check for leaks to verify that the microfluidic device has no defects and all tubing connections are sealed. Dispense water through the inlet tubes as needed with a syringe and monitor for any fluid leaking in the main channel.
    2. Dispense a known volume through the chip, and measure the volumes collected from the outlets to ensure that the flow ratio is as expected. Deviations from the expected volume ratio may indicate blockages in one of the outlets or leaking connections.
        1. To maintain system cleanliness and prevent clogging flush the entire system (fluidic tubing and chip) with appropriate cleaning solutions (*e.g.*, bleach, ethanol, water) before and after running any experiments.

2. In the event of clogs or blockages in one of the outlets, flush the system while plugging the clear outlet to clear the blockage. If this is unsuccessful, reverse the flow direction during flushing, optionally applying rapid pulses of reverse flow (using a manually-actuated syringe). Finally, if the blockage still cannot be removed, replace the tubing or chip, as necessary.

3. Frequency Scan Setup for Acoustic Focusing
   1. Fill the bypass channel (see **Figure 1**) with fluid such as deionized water, ethanol, or phosphate buffered saline (PBS) by manual injection with a syringe. Note that this fluid does not come into contact with the sample being processed. The details of adjusting node position using different bypass fluids are described elsewhere[16,17]. In brief, if the node needs to be closer to the dividing wall, use a lower-density bypass fluid, such as ethanol; for node placement closer to the input sample stream, choose a denser fluid, such as a glycerol solution.
   2. Make a bead solution of approximately 0.01% (w/v) 5–8 µm fluorescent polymer beads suspended in a buffer such as PBS with 0.05% Tween-20 and fill the sample inlet syringe with the bead solution. Fill the buffer inlet syringe with the same buffer (this does not need to be the same fluid as in the bypass channel). Note that in general, the buffer is chosen to suit the application (see Step 5.1).
   3. With the fluidic breadboard on the microscope stage, focus approximately halfway into the depth of the channel at a straight channel region just before the outlet with both channels (separation and bypass) in the field of view. An additional oblique-angle external light source may be required to make the channel walls visible, for successful post-processing of image data.

4. Automated Frequency Scan and Image Capture
   1. Make electrical connections using shielded cables (*e.g.*, RG-58 equipped with BNC connectors) to a function generator with radio frequency (RF) amplifier to deliver the excitation signal to the piezo transducer. Optionally, connect an oscilloscope to the output of the function generator for monitoring the actual voltage applied to the transducer.
   2. Turn on the cooling fan, and set the function generator such that the output of the RF amplifier to the piezo transducer is in the range of 12–25 volts peak-to-peak (V_{pp}).
   3. Set both syringes to the same flow rate between 50 and 200 µl/min. Using a single syringe pump to drive both syringes with the same motor is recommended to minimize perturbations to the flow.
   4. Perform a frequency scan procedure by specifying the start and end frequencies, the step size between frequency values, and the piezo drive voltage using a laboratory automation toolkit such as National Instruments LabVIEW.
   5. At each frequency step, apply the voltage for 15 sec to allow the system to equilibrate, then capture 10 images of beads flowing through the chip for subsequent analysis (exposure times between 10 and 100 msec are recommended).
   6. Between each applied frequency step, turn off the voltage for approximately 20 sec to let the beads redistribute uniformly across the channel and remove bias in focusing from the previously applied frequency step.

5. Image Analysis to Determine Resonant Frequency and Focusing Position
   1. Run an image analysis script (such as the AF_freqScanPlotter.m MATLAB script provided with this Protocol) and enter the required information at the prompts: select the list of image files generated in Step 4.4, enter the scan start and stop frequencies and step size, the full channel width, the wall location, and finally select the image region to analyze, including both the separation and bypass channels.
   2. Observe the analysis script average the set of images captured at each frequency step, and average the intensity values along the flow direction. This results in a cross-section line-scan of fluorescence intensity.
      NOTE: The frequency corresponding to the highest intensity is defined as the resonant frequency (**Figure 3**, middle row), and the position in the channel where the highest intensity occurs is the focusing position (**Figure 3**, bottom row).

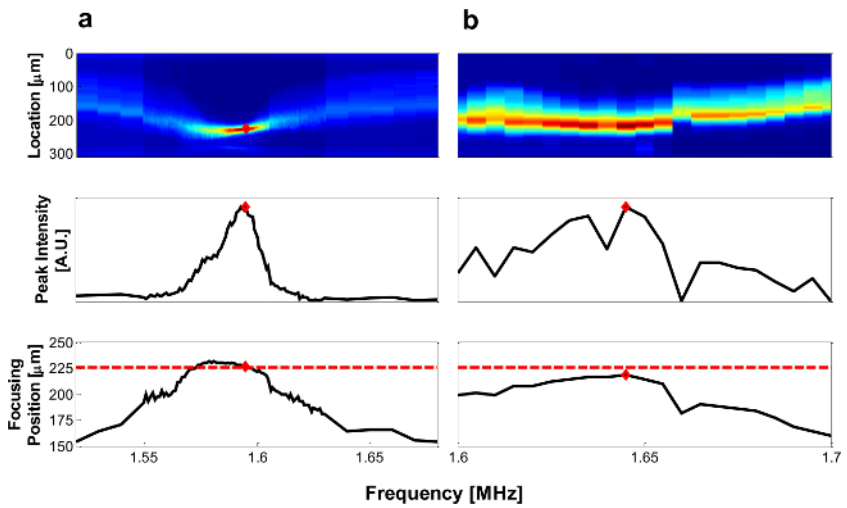

Figure 3. Representative Frequency Scan. Example of frequency scan data for well coupled (**A**) and poorly coupled (**B**) piezo and chip. Top row: fluorescent intensity of beads (red represents high, and blue represents low intensity). Middle row: maximum intensity at each frequency. Bottom row: location of maximum intensity, where the red dashed line indicates predicted focusing position, and red diamonds indicate resonant frequency as determined by the maximum intensity. Please click here to view a larger version of this figure.

5. Automated Separation

NOTE: The automated separation experiment is run to separate large particles from small particles due to the size-dependent acoustic focusing forces applied in the microfluidic chip. The required system components are grouped together in the Materials List.

1. System Configuration and Sample Preparation
    1. Connect the microfluidic chip to the syringe pump, computer-controlled multi-port selection valves, PC-interfaced flow meters, and tubing, as shown in **Figure 4**. This configuration enables automated processing of samples through the microfluidic separation chip, as well as automated cleaning steps between experiments to remove cross-contamination and sample carry-over.
    2. Use a sample buffer suitable for the cells or particles to be separated, or as required by the analysis assay to be used after separation. As in Step 4.3.2, the recovery buffer (but not necessarily the bypass fluid) must match the sample fluid.
    NOTE: Any aqueous buffers typically used with biological samples (*e.g.*, PBS) have acoustic properties similar to water and will not appreciably change the performance of the acoustic device. The use of sample fluids with density and viscosity significantly different from water is possible, but only recommended for operators with significant acoustophoresis experience.

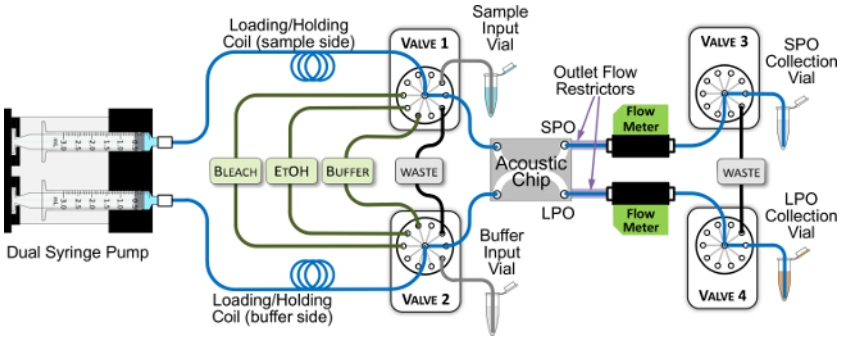

Figure 4. Acoustic System Configuration for Automated Separation Experiments. The blue lines trace the main flow path through the system. All green and black lines are 0.03" inner diameter (ID) tubing, and all blue and gray-colored lines are 0.01" ID tubing, with the exception of the holding coils, which are 0.03" ID, and the flow restrictors, which are 0.006" ID. The syringes are filled with buffer, and the holding coils have sufficient volume (550 µl) to prevent uptake of any samples or cleaning reagents into the syringes. Please click here to view a larger version of this figure.

2. Separation Procedure
    1. Pre-run state. Prior to running the separation, ensure that the cleaning reagent reservoirs (bleach, ethanol, buffer) have sufficient fluid, the waste reservoirs are not full, and the fluid lines are primed (*i.e.*, filled with solution). If the latter condition is uncertain, or if the system is being run for the first time after idling (*e.g.*, the first time on a given day), run an automated cleaning procedure (see Step 5.3 below). Set Valves 3 and 4 at the chip outlets to flow to waste reservoirs initially.
    2. Turn on the cooling fan, and set the function generator at the resonant frequency for the acoustic chip being used, as determined in step 4.5. Adjust the voltage set point on the function generator so that the RF amplifier outputs between 12 and 25 V_{pp}, as appropriate for the desired separation.
    3. Connect the Sample Input Vial, Buffer Input Vial, and appropriate collection vials to the system. Just before attaching the Sample Input Vial to its pickup tubing, vortex the vial briefly to re-suspend any particles that may have settled. Then, attach the vial and initiate the separation routine without delay.
    CAUTION: If the sample to be processed contains potentially infectious agents, the vials should be of a screw-top type, to maintain a sealed system and prevent sample aerosolization. In addition, when working with biohazardous materials, handle all vials and tubing while wearing the necessary protective equipment and using the required hazard controls and procedures for the Biological Risk Group and Biosafety Level appropriate to the material. Consult institutional policies and protocols in case of any uncertainty.
    4. Use a program in a laboratory automation toolkit to control the valves, flow sensors and pump to carry out the fully-automatic separation routine.
    NOTE: The routine switches the valves, actuates syringe pump withdrawal and infusion, and monitors flow sensor data for correctly timing the collection of output sample fractions. The major steps are summarized below in 5.2.4.1 through 5.2.4.3, as if carried out manually.
        1. Prime the pickup tubing. Withdraw approximately 15 µl from the Sample Input Vial to completely fill the tube connecting it to Valve 1. Simultaneously, prime the tube connecting the Buffer Input Vial to Valve 2. In a similar fashion, prime the air inlet of Valve 1 to ensure that it contains no fluid. Finally, switch Valves 1 and 2 to expel to waste any excess fluid or air that has entered the loading coil.
        2. Load the sample coil, as shown in **Figure 5a**. A typical loading sequence for processing a 250-µl sample is to withdraw 25 µl of air at 50 µl/min, then 250 µl of sample at 200 µl/min, followed by 35 µl of leading buffer at 200 µl/min, and finally another 25 µl of air at 50 µl/min.
        NOTE: All volumes and flow rates are user-selectable. Note that this loading sequence is in reverse order of how the fluid plugs will flow through the separation device.
        3. Begin sample infusion. Set the syringe pumps to infuse the loaded fluid plugs at the desired rate (typically 100 µl/min). Monitor the flow rates at the SPO and LPO with flow sensors to ensure that flow is steady and at the ratio determined in Step 4.1, and that clogging has not occurred.

4. Collect separated fractions. When the flow sensors detect a spike in flow rate, indicating passage of the first air gap, switch the corresponding output valve from waste (where it started in Step 5.2.1) to a sample collection vial.
5. After passage of sample from the chip, observe the flow sensor detect the second air gap. At this point, switch the output valves back to waste. After the full volume loaded from Step 5.2.4.2 is dispensed, stop the syringe pump infusion and terminate the automation routine when the flow rate reaches zero.

5. After the separation experiment is complete, disconnect the SPO and LPO sample collection vials and store them appropriately for subsequent analysis.

3. Automated Cleaning and Decontamination
NOTE: Before processing each sample, flush and decontaminate the whole fluidic system using the following automated routine.
1. Secure the SPO and LPO collection vial tubes, as well as the sample pickup tube in empty vials to collect excess cleaning solutions that will be flushed through the tubes.
2. Start the automated system cleaning routine. As with the Automated Separation procedure in Step 5.2, the program should control the valves and syringe pump to sequentially load the holding coil with cleaning reagents, and flush them through the system.
3. Perform the following cleaning routine: flush with 10% bleach, then with 70% ethanol, and end with water or an appropriate saline buffer (*e.g.*, 1x PBS or buffer used for sample processing). Use the following flush volumes: 450 µl for bleach and ethanol, and 1,000 µl for water/buffer.
4. During flushing steps, flush each reagent into the SPO while the LPO outlet valve is set to a port that is blocked, then vice versa, to remove any potential clogs in the outlet flow restrictors. Maintain withdrawal and infusion flow rates of 300–500 µl/min to minimize bubble generation in the tubing and backpressure buildup when either the SPO or the LPO is blocked.
5. Discard the excess flushing solutions and the vials in which they collected by following appropriate procedures for handling biological or chemical waste.

Representative Results

Key features of the acoustic-microfluidic device design are highlighted in **Figure 1**, and described fully elsewhere.[15] In brief, two fluid streams flow side-by-side in a separation channel, separated from a parallel bypass channel by a thin silicon wall. Since the primary radiation force magnitude scales with particle volume, large particles migrate out of the mixed-sample input stream toward the acoustic pressure node located in the adjacent recovery fluid stream, while small particles remain in the original stream (**Figure 1B**, **C**). The subdivided two-channel architecture improves particle separation[17] and allows adjustment of the node position by using different bypass channel fluids.[16] The fluidic breadboard and fixtures provides a robust platform for world to chip connections, and the modular design enables rapid changing between fluidic chips (**Figure 2**). This configuration likewise allows reversible fluid connections, which seal up to 1,000 psi, to be made quickly and reliably (**Figure 2B**, **E**).

The resonant frequency f_{res} of a chip can be estimated using simple 1D analytical calculations (refer to Step 1.1.1). From a more complete 2D finite-element model of our device cross-section,[16] the expected focusing position for 2-node resonance is 225 µm from the wall and the expected frequency is 1.68 MHz. However, f_{res} of real devices can vary by ±100 kHz, depending on operating temperature and coupling of longitudinal and lateral resonances. Therefore, after device assembly, f_{res} must be empirically verified at relevant flow rates and piezo drive voltages, as described in Step 4 of the protocol. **Figure 3** shows representative frequency scans taken at 200 µl/min, with water in the main and bypass channels, and 20 V_{pp} supplied to the piezo. When coupling between the piezo and microfluidic device is good, particles will focus tightly at the resonant frequency, resulting in a clear peak in the fluorescent intensity and migration to the expected focusing position (**Figure 3A**). In contrast, when there is poor coupling, particles will not focus well and the frequency scan results will be similar to **Figure 3B**. In such devices, the piezo transducer may need to be re-mounted, if a reversible adhesive has been used; otherwise, this device is unsuitable when high-quality focusing or fast flow are critical for the required application. The data in **Figure 3** inform the choice of operating frequency for subsequent experiments, and the voltage and flow rate range available for efficient particles separation.

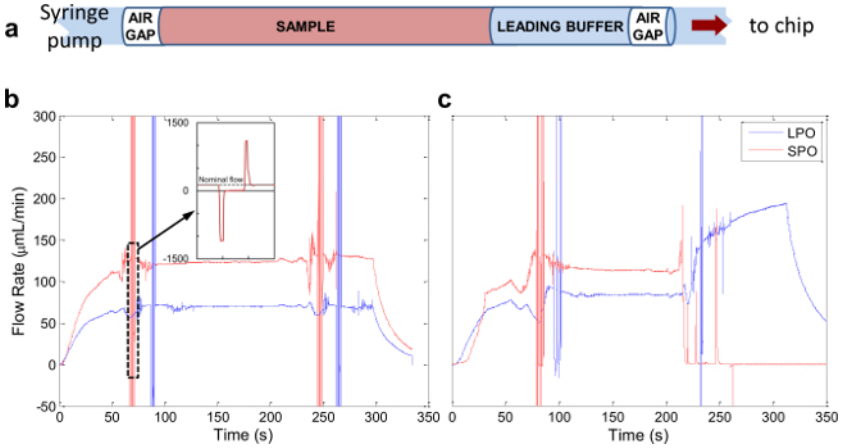

Figure 5. Automated Sample Processing. (**A**) Schematic of sample loaded in the sample coil. (**B**) Representative flow profile of a successful separation experiment. (**C**) Flow profile from a separation run during which the SPO outlet clogged at approximately 220 sec. Please click here to view a larger version of this figure.

After identifying chips that are effective separators, they are incorporated into the system depicted in **Figure 4**. Total system swept volume is minimized by using tubing with 0.01" inner diameter along the main flow path (blue lines). **Figure 5A** illustrates the make-up of a typical sample plug infused through the system. A small amount of "leading buffer" (~35 µl) is required to precede the sample in the flow to eliminate flow fluctuations while the sample is moving through the separation chip. **Figure 5B** shows flow data resulting from a successful automated acoustic separation experiment. Key features of a successful run include: (1) a transient increase in flow rate in both the LPO and SPO as pressure builds and fluid begins to flow through the system, (2) a sharp spike indicating the passage of an air bubble (the inset shows an expanded profile of a single bubble), which should reach the SPO before the LPO due to the unequal flow from the two outlets, (3) stable flow through both outlets between the two air bubbles as the sample moves through the system, and (4) a gradual decrease in flow rate in both outlets after the full sample volume is delivered to the system. Problematic runs are immediately apparent from flow profiles similar to **Figure 5C**, where it appears that the SPO became clogged after approximately 220 seconds. In this case, a cleaning procedure similar to that described in Step 5.3 should be run to unclog the channel.

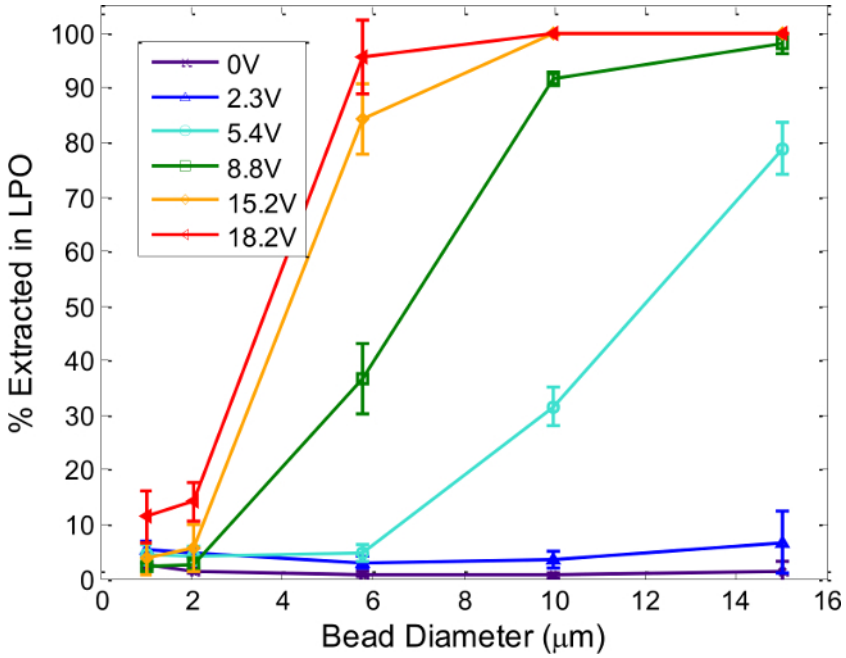

Figure 6. Device Tunability: Particle Size and Voltage Effects. Percent of polystyrene microspheres extracted in the LPO depends on the particle size and voltage supplied to the piezoceramic. Each line corresponds to a different operating voltage at the resonant frequency, determined as described in Step 4. Total flow rate through the device is 200 µl/min, with applied drive frequencies between 1.62 and 1.64 MHz. Error bars represent the standard deviation of at least three separate experiments. Reproduced and modified by permission of The Royal Society of Chemistry from http://pubs.rsc.org /en/Content/ArticleLanding/ 2014/AN/c4an00034j. Please click here to view a larger version of this figure.

Figure 6 shows compiled separation results using various polystyrene particle sizes and piezo driving voltages that demonstrate the operating parameters necessary for efficient separation. In general, higher voltages (*i.e.*, greater acoustic forces) are required to extract smaller particles, as expected. Drive voltages cannot be indefinitely increased, however, due to greater heat dissipation and increasing effects of acoustic streaming.[13] The plot serves as a general guide for particle separation—particle sizes that show significantly different recovery at a specific drive voltage (*e.g.*, 10- and 2-µm particles at 8.8 V_{pp}) will separate well. Generally, particle populations with a large size difference, such as viruses (~100 nm) and cells (~10 µm) can be separated rapidly and efficiently, as can cells of different sizes (*e.g.*, 6–8 µm discoidal erythrocytes and 8–15 µm leukocytes). The specific conditions required to work with other cell types must be empirically determined, as cell shape, density and compressibility affect its acoustic contrast, in addition to cell size. To this end, the procedures in Step 4 are useful for determining usable separation conditions for any new cell or particle type, and not only for assessing the quality of a particular acoustophoresis device.

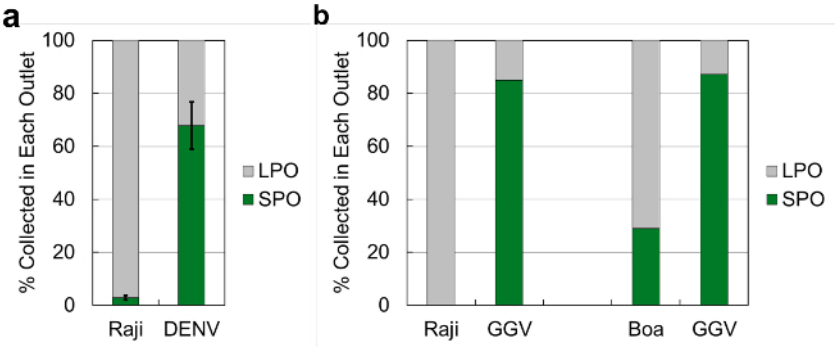

Figure 7. Separation Efficiency of Cell-Virus Spiked Samples. Separation results from (**A**) Raji cells spiked with Dengue virus (DENV) and (**B**) Raji cells and Boa kidney cells spiked with Golden Gate Virus (GGV). Percentages collected are defined as the fraction of viruses or cells exiting from a specific outlet compared to the total amount exiting the chip. The error bars for (**A**) are the standard deviation of 3 trials, whereas the samples in (**B**) were only processed once due to the low quantities available. 1x PBS was used as the sample buffer and recovery fluid, with water in the bypass channel for all experiments. Chip operating frequencies ranged between 1.60 and 1.64 MHz, with drive voltages between 16 and 20 V_{pp}. Please click here to view a larger version of this figure.

To demonstrate the utility of this platform for biological particle separation, we first used it to process well-characterized biological samples: human Raji cells (10^5 cells/ml, average diameter 8–10 μm[25]) spiked with dengue virus (DENV, 10^5 pfu/ml, approximate diameter 50 nm[26]). **Figure 7A** shows the percentage of Raji cells and DENV collected in both the SPO and LPO (defined as the fraction of each particle type collected from each outlet compared with the total amount of each particle collected from the chip). The experiment was repeated in triplicate, and Raji cells were quantified using a Coulter counter, while DENV was quantified using a reverse-transcription quantitative polymerase chain reaction (RT-qPCR).

Next, the performance of the system was tested in a scenario that is more realistic for processing clinical samples, in which the exact physical characteristics of the particles may be unknown, and the available sample quantities are lower. Here, we assessed separation of the recently-identified golden gate virus (GGV), a snake pathogen infecting boa constrictor kidney cells.[27] The size of the GGV virus particle has not yet been measured, but since GGV belongs to the *Arenaviridae* family, it is likely of a similar size, between 100 and 150 nm.[28] We processed samples with GGV spiked (10^4 pfu/ml) into Raji human cells (not an infection target for the virus), and boa kidney cells (infection target for GGV, approximate size 10 μm[27]), with both cell types at 10^4 cells/ml. As these samples were available in low quantities, separation results from only one experimental run are reported in this work. **Figure 7B** shows the percentage of Raji cells, Boa cells, and GGV collected from the SPO and LPO. Cells were quantified in these experiments by counting on a hemacytometer and viruses were quantified by RT-qPCR.

Discussion

This protocol presents the system-level integration of microfluidic devices to macroscale equipment to perform automated biological sample processing. The modularity of this platform allows it to be adaptable to any continuous flow device, and, as an example, the presented protocol focuses on characterizing and optimizing the performance of an acoustofluidic particle separation device. Three major advantages of this protocol are highlighted: (i) modularity and chip-to-world interfacing, (ii) robust characterization of device performance, and (iii) automated processing of precisely metered sample volumes for particle separation.

i. Modularity and chip-to-world interfacing

As shown in **Figure 2**, the microfluidic chip is mounted on a custom breadboard to easily fit onto a microscope stage for direct observation. The breadboard contains #6-40 UNF threaded holes on a 5 mm-pitch grid, enabling the chip to be secured, and fluid connections to be made. The fluid connections are PEEK tubes with machined ends, which seal against the fluidic chip with a rubber face-sealing gasket and a stainless steel collar. This interface scheme makes for easy chip replacement and rapid device redesign, requiring few or no changes to other system components, provided chip footprints conform to the grid format. For example, we have used this platform with microfluidic chips for continuous-flow electrophoresis, thermal cell lysis,[29] rapid mixing of reagents for chemical synthesis, and single-cell capture and interrogation.

ii. Robust characterization of device performance

In order to optimize the performance of any microfluidic separation device, its operation must first be thoroughly characterized. The system described here supports the development of rapid and automated protocols to do this. For the specific example of acoustic focusing devices, the focusing quality, operating frequency, and position of focused particles in the microfluidic channel must be measured for each individual device. These measurements require sweeping through a range of piezoceramic drive frequencies, voltages and flow rates, to identify the optimal parameter combinations for high-quality separation. The presented protocol automatically varies these tunable parameters and captures the relevant data—*i.e.*, fluorescent images of particles flowing in the channel that are post-processed to generate the required measurements of particle focusing quality, frequency, and position (**Figure 3**).

Full characterization of acoustic device performance requires repeating Steps 4.4 and 4.5 as needed under different experimental conditions. For instance, the absolute focusing position of a chip is found by running the frequency scan at relatively low flow rates and high voltages to ensure complete migration to the node location. Additionally, such frequency scans can assess the quality of device assembly (when run with polystyrene beads of known size), or to determine how a previously-unknown particle type will behave in the system (after a chip has been characterized with beads). A chip with good energy transfer from the piezoceramic to the microfluidic channel will result in tight focusing at high flow rates (>1 ml/min) and low voltages (12–15 V_{pp}), while those with poor energy transfer will not focus even at low flow rates (<100 μl/min) and

high voltages (>20 V_{pp}). We have found that intimate contact between the microfluidic chip and the piezoceramic is critical for efficient energy transfer into the fluid. Further investigation of the optimal method of bonding the microfluidic chip and the piezoceramic will enable reliable production of high-performance devices.

Finally, a complete picture of an acoustophoretic device's operation can be obtained by combining the image-based frequency scan measurements of Step 4 (and **Figure 3**) with particle counts collected from the SPO and LPO as functions of the relevant operating parameters, from separation experiments carried out with microspheres, as described in Step 5. As shown in **Figure 6**, such a series of automated experiments can rapidly characterize an individual device's performance and tunability, informing the user of the optimal parameter space to operate the device for particle separation.

iii. Automated small-sample processing for particle separation

For successful and accurate microfluidic chip-based sample processing, it is critical to reliably and precisely meter, load, deliver, and collect the volumes of fluid as they pass through. This precision is especially important when the sample volume is small (~0.1–1 ml), which is common in clinical or research laboratory settings.[30] Precise sample handling is challenging in traditional microfluidic experiments that employ manual withdrawal of the sample into a syringe and infusion into a device with no feedback of when the sample has been separated and when it should be collected. The presented protocol employs automated sample coil loading and dispensing coupled with real-time feedback from flow sensors to enable reproducible separations of small sample volumes.

Figure 5 shows the flow profiles measured at the SPO and LPO from a typical separation experiment. First, leading buffer of at least 35 µl is loaded to ensure stable flow before the sample reaches the acoustic chip. Sample volumes less than 100 µl are not recommended for this system configuration, because sample dilution due to the leading buffer becomes excessive. A plug of air is used at the beginning of the injection before the leading buffer to separate the sample plug from the fluid that follows, preventing mixing and dilution of sample and serving as an indicator to the flow sensors. After an initial transient as fluid begins moving through the system, sharp spike signals in both outlets indicate the passage of the first air bubble. These transients are followed by a long period of stable flow as the sample flows through the system, then another spike when the second air bubble passes, and finally an eventual decrease in flow rate to zero after the syringe pump stops.

The passage of the air plugs through the flow sensors is used as trigger points to switch the valves to start and stop sample collection, thus minimizing lost sample and dilution by non-sample fluid volumes. Closed-loop metering of processed sample volumes eliminates the need to re-program these values prior to the start of the experiment each time the input sample is changed. This feature is particularly important when sample volume is limited, for example in the case of many clinical samples. Real-time flow monitoring also assists in troubleshooting; a poor run (*e.g.*, a clog forming in one of the outlets) is immediately evident from the resultant flow profiles, as in **Figure 5b**.

To demonstrate the flexibility and effectiveness of acoustofluidic separation using the presented system architecture, purified DENV and GGV virus stocks were spiked into cell stocks and separated by processing through the microfluidic chip. **Figure 7a** shows that Raji cells were well-separated from viruses, as 97% of Raji cells exiting the chip were found to be in the LPO, thereby leaving a highly enriched sample of DENV in the SPO. In comparison, the efficiency of DENV separation was lower, with 70% of DENV exiting the chip found in the SPO. This can be attributed to slight convective mixing induced by the turns of the separation channel, but more likely to some DENV particles migrating along with the Raji cells into the LPO. Cells migrating laterally across streamlines drag some fluid with them, even at low Reynolds number. By this mechanism, as well as nonspecific surface adsorption, viral particles transfer into the LPO. Nevertheless, the highly enriched sample of DENV in the SPO is a significant benefit, for instance when *de novo* sequencing is used to detect and identify viruses.

Figure 7b shows that in one experimental run, only about 70% of Boa cells exiting the chip were found in the LPO, compared with nearly 100% separation efficiency for Raji cells. The difference in separation performance between the two cell types may be attributable to a smaller average size or a lower density of Boa cells as compared to Raji cells, therefore resulting in smaller acoustic forces. To confirm or refute these suppositions, the size, density and morphology of Boa cells in suspension (which normally grow adherent) of Boa cells must be accurately measured, an effort for further investigation. In the same experiments, similarly to the experiments with DENV, the bulk of the recovered GGV exited from the SPO, indicating an enrichment of the viral fraction.

The presented data highlight the inherent challenges of engineering broadly-applicable platforms for processing a variety of biological samples. Importantly, the biological interactions can begin to play as great a role as the physical and mechanical effects. However, these preliminary experiments also demonstrate the power and promise of using this system architecture for sample processing in clinical and research applications. As a robust, well-characterized engineered system, this platform provides the capability to seek answers to new scientific questions.

Disclosures

The authors have nothing to disclose.

Acknowledgements

This work was performed under the auspices of the U.S. Department of Energy by Lawrence Livermore National Laboratory under Contract DE-AC52-07NA27344, and partially supported by LLNL's Laboratory Directed Research and Development (LDRD) program, 14-LW-077. The authors thank Michael Wilson, Mark Stenglein and Joe DeRisi at the Univeristy of California, San Francisco for generously providing GGV and Boa cell samples. EJF acknowledges support from the LLNL Lawrence Scholar Graduate Program. MS acknowledges support from the UC Office of the President Lab Fees Research Program. LLNL-JRNL-665235

References

1. Gossett, D. R., Weaver, W. M., *et al.* Label-free cell separation and sorting in microfluidic systems. *Analytical and Bioanalytical Chemistry.* **397** (8), 3249–3267, doi:10.1007/s00216-010-3721-9 (2010).
2. Lenshof, A., & Laurell, T. Continuous separation of cells and particles in microfluidic systems. *Chemical Society Reviews.* **39** (3), 1203–1217, doi:10.1039/b915999c (2010).
3. Sajeesh, P., & Sen, A. K. Particle separation and sorting in microfluidic devices: a review. *Microfluidics and Nanofluidics.* **17** (1), 1–52, doi:10.1007/s10404-013-1291-9 (2014).
4. Bhagat, A. A. S., Bow, H., Hou, H. W., Tan, S. J., Han, J., & Lim, C. T. Microfluidics for cell separation. *Medical & Biological Engineering & Computing.* **48** (10), 999–1014, doi:10.1007/s11517-010-0611-4 (2010).
5. McGrath, J., Jimenez, M., & Bridle, H. Deterministic lateral displacement for particle separation: a review. *Lab Chip.* **14** (21), 4139–4158, doi:10.1039/C4LC00939H (2014).
6. Jubery, T. Z., Srivastava, S. K., & Dutta, P. Dielectrophoretic separation of bioparticles in microdevices: A review. *ELECTROPHORESIS.* **35** (5), 691–713, doi:10.1002/elps.201300424 (2014).
7. Jin, C., McFaul, S. M., *et al.* Technologies for label-free separation of circulating tumor cells: from historical foundations to recent developments. *Lab on a Chip.* **14** (1), 32, doi:10.1039/c3lc50625h (2014).
8. Trujillo, F. J., Juliano, P., Barbosa-Cánovas, G., & Knoerzer, K. Separation of suspensions and emulsions via ultrasonic standing waves – A review. *Ultrasonics Sonochemistry.* **21** (6), 2151–2164, doi:10.1016/j.ultsonch.2014.02.016 (2014).
9. Bridle, H., Miller, B., & Desmulliez, M. P. Y. Application of microfluidics in waterborne pathogen monitoring: A review. *Water Research.* **55**, 256–271, doi:10.1016/j.watres.2014.01.061 (2014).
10. Mariella, R., Jr Sample preparation: the weak link in microfluidics-based biodetection. *Biomedical microdevices.* **10** (6), 777–784, doi:10.1007/s10544-008-9190-7 (2008).
11. Gor'kov, L. P. On the forces acting on a small particle in an acoustic field in an ideal fluid. *Soviet Physics - Doklady.* **6**, 773–775 (1962).
12. Settnes, M., & Bruus, H. Forces acting on a small particle in an acoustical field in a viscous fluid. *Physical Review E.* **85** (1), 016327, doi:10.1103/PhysRevE.85.016327 (2012).
13. Barnkob, R., Augustsson, P., Laurell, T., & Bruus, H. Acoustic radiation- and streaming-induced microparticle velocities determined by microparticle image velocimetry in an ultrasound symmetry plane. *Physical Review E.* **86** (5), doi:10.1103/PhysRevE.86.056307 (2012).
14. Bruus, H. Acoustofluidics 7: The acoustic radiation force on small particles. *Lab Chip.* **12** (6), 1014–1021, doi:10.1039/C2LC21068A (2012).
15. Fong, E. J., Johnston, A. C., *et al.* Acoustic focusing with engineered node locations for high-performance microfluidic particle separation. *Analyst.* **139** (5), 1192–1200, doi:10.1039/C4AN00034J (2014).
16. Fong, E. J., Bora, M., *et al.* Continuously Variable Node Position in a High-Throughput Acoustofluidic Device. *Micro Total Analysis Systems* , 1184–1186 (2014).
17. Jung, S.-Y., Notton, T., Fong, E., Shusteff, M., & Weinberger, L. S. Spatial tuning of acoustofluidic pressure nodes by altering net sonic velocity enables high-throughput, efficient cell sorting. *Lab on a Chip.* **15** (4), 1000–1003, doi:10.1039/C4LC01342E (2015).
18. Franssila, S. Deep Reactive Ion Etching. *Introduction to Microfabrication*. 255–270 at <http://onlinelibrary.wiley.com/doi/10.1002/9781119990413.ch21/summary> (2010).
19. Sharma Rao, B., & Hashim, U. Microfluidic Photomask Design Using CAD Software for Application in Lab-On-Chip Biomedical Nanodiagnostics. *Advanced Materials Research.* **795**, 388–392, doi:10.4028/www.scientific.net/AMR.795.388 (2013).
20. Melin, J., & Quake, S. R. Microfluidic Large-Scale Integration: The Evolution of Design Rules for Biological Automation. *Annual Review of Biophysics and Biomolecular Structure.* **36** (1), 213–231, doi:10.1146/annurev.biophys.36.040306.132646 (2007).
21. Madou, M. J. *Fundamentals of microfabrication: the science of miniaturization.* CRC Press: Boca Raton. (2002).
22. Krulevitch, P., Benett, W., Hamilton, J., Maghribi, M., & Rose, K. Polymer-based packaging platform for hybrid microfluidic systems. *Biomedical Microdevices.* **4** (4), 301–308 (2002).
23. Leslie, D. C., Easley, C. J., *et al.* Frequency-specific flow control in microfluidic circuits with passive elastomeric features. *Nature Physics.* **5** (3), 231–235, doi:10.1038/nphys1196 (2009).
24. Oh, K. W., Lee, K., Ahn, B., & Furlani, E. P. Design of pressure-driven microfluidic networks using electric circuit analogy. *Lab on a Chip.* **12** (3), 515–545, doi:10.1039/C2LC20799K (2012).
25. Mittelbrunn, M., Gutiérrez-Vázquez, C., *et al.* Unidirectional transfer of microRNA-loaded exosomes from T cells to antigen-presenting cells. *Nature Communications.* **2**, 282, doi:10.1038/ncomms1285 (2011).
26. Acosta, E. G., Castilla, V., & Damonte, E. B. Functional entry of dengue virus into Aedes albopictus mosquito cells is dependent on clathrin-mediated endocytosis. *Journal of General Virology.* **89** (2), 474–484, doi:10.1099/vir.0.83357-0 (2008).
27. Stenglein, M. D., Sanders, C., *et al.* Identification, Characterization, and *In Vitro* Culture of Highly Divergent Arenaviruses from Boa Constrictors and Annulated Tree Boas: Candidate Etiological Agents for Snake Inclusion Body Disease. *mBio.* **3** (4), e00180–12–e00180–12, doi:10.1128/mBio.00180-12 (2012).
28. CDC. *Arenaviridae* | Viral Hemorrhagic Fevers (VHFs) | CDC *http://www.cdc.gov/vhf/virus-families/arenaviridae.html.* (2013).
29. Packard, M., Wheeler, E., Alocilja, E., & Shusteff, M. Performance Evaluation of Fast Microfluidic Thermal Lysis of Bacteria for Diagnostic Sample Preparation. *Diagnostics.* **3** (1), 105–116, doi:10.3390/diagnostics3010105 (2013).
30. Lion, N., Reymond, F., Girault, H. H., & Rossier, J. S. Why the move to microfluidics for protein analysis? *Current Opinion in Biotechnology.* **15** (1), 31–37, doi:10.1016/j.copbio.2004.01.001 (2004).